EFFECT OF METAL SEQUESTRANTS ON THE DECOMPOSITION OF HYDROXYLAMMONIUM NITRATE

BY

EMIL JONAS BROEMMELSIEK

THESIS

Submitted in partial fulfillment of the requirements
for the degree of Master of Science in Aerospace Engineering
in the Graduate College of the
University of Illinois Urbana-Champaign, 2021

Urbana, Illinois

Adviser:

Associate Professor Joshua L. Rovey

ABSTRACT

Hydroxylammonium nitrate (HAN) is an energetic salt used in flight-proven green monopropellants such as ASCENT (formerly AF-M315E) flown in NASA's 2019 Green Propellant Infusion Mission and SHP163 flown in JAXA's Rapid Innovative Satellite Technology Demonstration-1. Decomposition of HAN is catalyzed by metals commonly found in storage tanks, a factor limiting its use. This work investigates the ability of metal-sequestering chelating agents to inhibit the de-composition of HAN. Isothermal and dynamic thermogravimetric analysis (TGA) were used to find isothermal decomposition rates, decomposition onset temperatures, and first-order Arrhenius re-action rate parameters. 2,2'-bipyridine (Bipy), triethanolamine (TEA), and ethylenediaminetetraacetic acid (EDTA) were studied as 0.05, 0.1, 0.5, 1, and 5% by weight additives in 90% aqueous HAN by weight. An isothermal decomposition rate of 0.137%/hr at 348 K was observed for HAN. Addition of 1% Bipy and 1% TEA reduced the isothermal decomposition rate by 20.4% to 0.109%/hr and by 3.65% to 0.132%/hr, respectively, showing that Bipy can inhibit decomposition. The addition of 1% EDTA increased the isothermal decomposition rate by 12.4% to 0.154%/hr. Bipy was found to increase the decomposition onset temperature from 454.8 K to 461.8 K while TEA and EDTA returned inconclusive changes. First order reaction rates calculated by the Ozawa-Flynn-Wall method were found to be insufficient to capture the effects of the additives tested. Bipy was found to inhibit the decomposition of HAN, while TEA and EDTA produced little or negative effect, a result believed to be due to poor metal complex stability at low pH and high acidity, respectively. Spectrophotometry was used for colorimetric analysis of Bipy+iron complexes and

showed that Bipy forms chelate complexes with trace iron impurities when added to HAN solutions.

TABLE OF CONTENTS

CHAPTER 1: INTRODUCTION

Hydroxylammonium Nitrate (HAN) based propellants have been recently flight-tested on multiple spacecraft [1] [2] and have been the subject of research for decades due to an array of useful properties, including but not limited to high density, high specific impulse, low freezing point, and low toxicity [3] [4] [5] [6] [7] [8] [9] [10] [11]. HAN's low decomposition temperature and ready catalysis has generated interest in energetic materials researchers toward studying its decomposition mechanism [12] [13] [14] [15] [16]. Catalytic decomposition and compatibility studies have found that transition metals have catalytic effects on low-temperature decomposition [3] [17]. This includes common elements like iron that can elute from metallic storage containers.

While catalyzing decomposition is desirable in a combustion chamber, it is not desirable in a storage tank. Tank materials can be changed, however the current state of the art procedure for synthesizing HAN results in part-per-million concentrations of metal impurities that still have a catalytic effect [12]. Sequestering metal ions in metal complexes reduces their catalytic activity [18] [19], which can inhibit the decomposition rate of propellants. Chelating agents are used for their metal-binding ability in a variety of applications including chemical manufacturing, food, medicine, cosmetics, and more [20] [21] [22] [23] [24]. Chelating agents are ligand molecules capable of forming stable, multidentate chelate complexes with metal ions, effectively sequestering the ion from reacting further [20]. One such molecule, N,N'-disalicylidene-1,2-propanediamine, is known as Metal Deactivator Additive (MDA) and has been studied for use as

a stabilizing additive in aviation fuels [18] [25]. MDA is not used in this study because it is soluble in non-polar oils and solvents (e.g. hydrocarbon fuels), but it is not soluble in water.

HAN is a salt with chemical formula $[NH_3OH][NO_3]$ that separates into hydroxylammonium (NH_3OH^+) and nitrate (NO_3^-) ions in solution according to R1:

$$HAN \rightleftharpoons NH_3OH^+ + NO_3^-. \quad \text{(R1)}$$

proton transfer between these two molecules, according to R2 and R3, controls the concentration of H^+ in HAN solution and thereby the pH of the solution:

$$HNO_3 \rightleftharpoons NO_3^- + H^+ \quad \text{(R2)}$$

$$NH_3OH^+ \rightleftharpoons NH_2OH + H^+. \quad \text{(R3)}$$

HAN has a high acidity and low pH because HNO_3 is a strong acid and NH_2OH is not a strong base. The proton transfer mechanism was found to be the most sensitive mechanism affecting HAN decomposition. Experiments done by Zhang found that adding HNO_3 until the concentration of H^+ was quintupled increased the overall decomposition rate by roughly 50 times while reducing the concentration of H^+ by adding NH_2OH reduced the overall rate of HAN decomposition [6]. Excess H^+ available in solution allows for the accumulation of additional NH_3OH^+ and NO_2^+ by R3 and R4, respectively, leading to the formation of decomposition products H_2O and N_2O as shown by Zhang's nitration/nitrosation pathway (R4-R8) [6]:

$$H^+ + HNO_3 \rightleftharpoons NO_2^+ + H_2O. \quad \text{(R4)}$$

$$NH_3OH^+ + NO_2^+ \rightarrow HONO + HNO + 2H^+ \quad \text{(R5)}$$

$$H^+ + HONO \rightleftharpoons NO^+ + H_2O \quad \text{(R6)}$$

$$NH_3OH^+ + NO^+ \rightarrow N_2O + H_2O + 2H^+ \quad \text{(R7)}$$

$$HNO + HNO \rightarrow N_2O + H_2O. \quad \text{(R8)}$$

This decomposition pathway also gives a mechanism for HAN autocatalysis since the number of H^+ produced by these reactions is higher than the number of H^+ required to start them. The more classical reduced kinetic model of Lee and Litzinger [5] includes R9, which is analogous to R4, citing it as the most dominant pathway for HNO_3 decomposition:

$$HNO_3 \rightleftharpoons NO_2^+ + OH^-. \quad \text{(R9)}$$

Chelating additives may affect the decomposition of HAN through two different mechanisms, and it is important to separate their effects. The initiation of decomposition of HAN requires available H^+. While chelating additives may sequester metallic ions and slow the decomposition rate, they may also change the catalytic activity of the H^+ concentration. Chelating additives are molecular species that may either dissociate to add more H^+ to the HAN solution or combine with H^+ to remove it through acid dissociation and recombination. R2 is an example of acid dissociation and recombination of a HNO_3 molecule. The change in H^+ concentration can be measured as a change in acidity (pH) of the solution. Both metal chelation and H^+ concentration change the decomposition rate of HAN. To isolate the effect of metal chelation on decomposition rate, the acidity of HAN solutions with chelating additives must be monitored.

Chelating additives may also decrease the decomposition rate of HAN by sequestration of metal ions. Metal ions catalyze the decomposition of HAN by assisting in oxidation of HAN through reactions such as R10, a dihydroxylamine ($NH(OH)_2$) formation proposed by Hansen et al. [3]. This reaction occurs especially when the metal atom is one that readily changes its oxidation state such as iron or copper. In R10, the iron ion is reduced from its 3+ oxidation state to its 2+ oxidation state and the hydroxylamine gains an oxygen, turning into dihydroxylamine:

$$NH_2OH \cdot HNO_3 + 2Fe(NO_3)_3 + H_2O \rightarrow NH(OH)_2 + 3HNO_3 + 2Fe(NO_3)_2. \quad \text{(R10)}$$

Surplus nitric acid is produced in R10 and may further contribute to HAN decomposition by increasing the solution acidity or through reactions like R11 and R12. For a trace amount of iron to contribute to HAN decomposition, the Fe^{2+} ions must be oxidized back to the Fe^{3+} ion by losing an electron so that they can be recycled to participate in R10 again. Hansen et al. [3] propose a method of iron oxidation that uses available nitrate ions and contributes to the production of product species nitric oxide and water, given as R11:

$$3Fe^{2+} + NO_3^- + 4H^+ \rightarrow 3Fe^{3+} + NO + 2H_2O. \quad \text{(R11)}$$

Hansen et al. propose another iron oxidation mechanism where the Fe^{2+} reacts with HAN, reducing the hydroxylammonium ion into an ammonium ion, while oxidizing the Fe^{2+} into Fe^{3+} [3]. Reaction R12 prepares the iron ions to participate once again in R10 and contributes to the decomposition of the HAN components into product species such as water and ammonia:

$$NH_2OH \cdot HNO_3 + 2Fe(NO_3)_2 + 2HNO_3 \rightarrow NH_4NO_3 + 2Fe(NO_3)_3 + H_2O. \quad \text{(R12)}$$

R10, R11, and R12 together are proposed by Hansen et al. as part of an explanation for the autocatalytic behavior of HAN [3]. In the presence of even trace quantities of metal ions, this set of reactions may recycle metal ions as a reactive species capable of breaking apart HAN at every step. In addition to the direct contribution to HAN decomposition by reaction with metal ions, the dihydroxylamine species produced in R10 is unstable and undergoes disproportionation as shown in R13 or R14:

$$2NH(OH)_2 \rightarrow N_2O + 3H_2O, \quad \text{(R13)}$$

where the product species nitrous oxide and water are formed, or:

$$2\mathrm{NH(OH)_2} + \mathrm{HNO_3} \rightarrow \mathrm{NH_2OH \cdot HNO_3} + \mathrm{HNO_2} + \mathrm{H_2O}, \quad \text{(R14)}$$

where nitrous acid is produced that increases the solution acidity and thereby catalyzes HAN decomposition.

The aim of this study is to determine if chelating agent additives influence the decomposition of HAN. Reactions R10, R11, and R12 illustrate part of a metal-catalyzed decomposition mechanism that may be inhibited by chelating additives, motivating the use of these additives in this work. With a systematic approach using multiple thermal analysis methods and isolating the effects of changes in pH, we show for the first time the effect of chelating agents on neat HAN with trace metal impurities and no additional user-added metals. These trace metals impurities are measured by ICP-MS and the iron content is confirmed by colorimetric analysis. This is the first body of work to investigate chelating agent effects on single part-per-million order metal concentrations. Previous work has investigated user-added metals on the order of 100 parts-per-million [13] [15]. Effects on decomposition are evaluated using thermogravimetric analyses (TGA) to calculate decomposition temperature, isothermal decomposition rate, and first order Arrhenius reaction rates to compare propellant samples with and without chelating agent additives. This work shows for the first time that Bipy inhibits the decomposition of HAN at 348 K and atmospheric pressure. Additionally, iron and other impurities are found in trace quantities in neat, unadulterated HAN.

CHAPTER 2: MATERIALS AND METHODS

2.1. CHEMICALS

HAN was acquired from Digital Solid State Propulsion in Reno, NV as a 45-47% by weight aqueous solution. It was concentrated using a rotary evaporator with a water bath set no higher than 323 K. Then isopropanol is added forming an azeotrope to assist in the evaporation of water from hygroscopic HAN. The HAN was then crystallized under low vacuum before adding a known quantity of deionized water to produce aqueous samples of 90%wt. HAN. For a detailed procedure on drying and crystallizing HAN, see Rasmont's thesis [26]. The 90% HAN produced for this study was measured to have a mass density of 1.599 g/mL with a standard deviation of 0.033 g/mL. Care was taken to use glass and polymer containers, pipettes, and probes to reduce contact with metals and prevent further metal contamination of the samples. Using a Sartorius QUINTIX1250-1S scale accurate to 10 μg, chelating agent additive was added to 90% HAN solution in 0.05, 0.1, 0.5, 1, and 5% by weight quantities.

Ethylenediaminetetraacetic acid (EDTA), triethanolamine (TEA), and 2,2' bipyridine (Bipy) were chosen to be tested as propellant additives to HAN solutions. EDTA (99.4-100.6%), TEA (>=99%), and Bipy (>99.7%) were purchased from Sigma-Aldrich (now Millipore Sigma). EDTA was chosen for its high complex formation stability constants with many species of metals [20] [27] and the latter two were chosen for their ability to form coordinate complexes with iron [20] [19] [28]. Iron is expected to be one of the most common impurities and among the most effective catalysts for HAN decomposition [12] [13] [4]. Iron (99.9%) and copper (98%) powders with grain sizes of less than 25 μm were purchased from Sigma-Aldrich.

2.2. INSTRUMENTATION

Metal impurities in unadulterated HAN were analyzed by Inductively Coupled Plasma Mass Spectrometry (ICP-MS). Raw HAN as received in 45-47% solution was analyzed for trace metal contents using a PerkinElmer NexION 350D ICP-MS system available through the UIUC School of Chemical Sciences Microanalysis Lab. Complexes of Bipy with some transition metals absorb light between 300 and 800 nm wavelengths [28] [29]. Light absorbance in the visible spectrum was measured using a Varian Cary 5G spectrophotometer at 1 nm detection intervals. A Hanna Instruments HI98100 pH checker with accuracy of ±0.2pH was used to measure pH of propellant samples.

Thermogravimetric analysis (TGA) is the methodology and equipment for measuring the mass of a sample continuously under a controlled temperature and atmosphere. Isothermal TGA is a constant temperature hold process wherein the mass of the sample is measured as a function of time. Dynamic TGA is a controlled heating process wherein the temperature of the environment and sample is increased at a prescribed rate and the mass of the sample is measured as a function of time. TGA data were acquired using a TA Instruments Q50 machine available at the Frederick Seitz Materials Research Laboratory (MRL) at the University of Illinois. The Q50 has a mass sensitivity of 0.1 μg and isothermal temperature accuracy of ±1°C. A 10 μL volumetric pipette was used to dispense samples to keep the sample weight at 15±2 mg. Isothermal data were acquired at 348 K and dynamic TGA was performed using 2, 5, 10, 15, and 20 K/min constant heating rates. Each TGA acquisition was done under a nitrogen atmosphere flowing across the sample at 60 mL/min. For a 15 mg sample representative of the constant heating ramp data, the error in mass percent is 0.0006 %wt. For a 30 mg sample representative of the isothermal data, the error in mass percent is 0.0003 %wt.

CHAPTER 3: RESULTS

3.1. METAL IMPURITY CONCENTRATION

Trace metals are present in the tested samples at sub-ppm levels. An estimate of the trace metal impurities in raw 45-47%wt HAN-water reagent was measured with ICP-MS. ICP-MS is a semi-quantitative technique with part-per-trillion detection limits for most metals. A rigorous quantitative process for measuring trace metal concentration with ICP-MS requires the use of standards with known concentration of each metal species. After measuring each standard, a calibration ratio of the measured element concentration to the actual concentration can be found for each element. Instead of pursuing a calibration for each metal, we used a single measurement for element identification, settling for speciation and an estimate of concentration approximate to an order of magnitude. The resulting metal concentration estimates with detected concentrations higher than 0.1 part-per-million are shown in Table 1.

Iron and copper are both known to catalyze the decomposition of HAN [3] [12] and both are detected in the raw HAN-water sample at 0.49 ppm and 0.1 ppm, respectively, as shown in Table 1. These same metal species are assumed to be present in the concentrated and crystallized HAN, and subsequently the 90%wt HAN-water and additive samples. This assumption is reasonable because metals exhibit orders of magnitude lower vapor pressures compared to water and evaporate very slowly even under vacuum. Thus, the expected metal concentrations in prepared 90% aqueous HAN samples are approximately twice the values of concentration measured in a 45% aqueous HAN sample. While iron and copper are thought to be the most catalytic impurities, Hansen et al. found that other metal species had a significant effect on the

decomposition of their HAN-based propellant samples [3]. These metals include titanium (Ti), tin (Sn), molybdenum (Mo), and vanadium (V), all elements detected by ICP-MS in this study.

Table 1. Elemental concentration detected by ICP-MS of 45-47%wt. HAN solution, ppm.

Element	Raw HAN
Cu	**0.10**
Zn	0.26
Ca	5.07
Fe	**0.49**
Na	5.88
Mg	0.18
Ti	0.39
Al	2.01
Ba	0.21
Mo	0.73
Se	0.75
Mn	0.54
V	0.23
Ni	0.37
Sn	1.91
Si	5.35
As	0.28

3.2. SAMPLE ACIDITY

The measured pH of propellant samples is shown in Figure 1. Sample pH was measured 48 hours after preparation to allow the sample to equilibrate. The error of each pH measurement, including the no-additive baseline, is the instrument measurement error of 0.2 pH. HAN was found to be highly acidic with the 90%wt HAN sample without additives having a pH of 2.8. This is to be expected since nitric acid is a strong acid and hydroxylamine is not a strong base.

Additives modify the pH, and the greatest effect is found for relatively high additive concentration. HAN with additives EDTA and TEA has a pH that is on average 3.0 and 3.1, respectively, for concentrations that are at or below 1%. HAN with additive Bipy has pH that is on average 2.7 for additive concentrations at or below 1%, and of the three additive samples studied it has pH closest to pure HAN-water. At additive concentrations at or below 1%, the pH is relatively constant for each sample deviating by at most 3% from the average. At relatively high concentration (5%), the pH significantly changes for all three samples. Specifically, for EDTA, the pH decreases to 1.7, for TEA it increases to 3.4, and for Bipy the pH increases to 3.3.

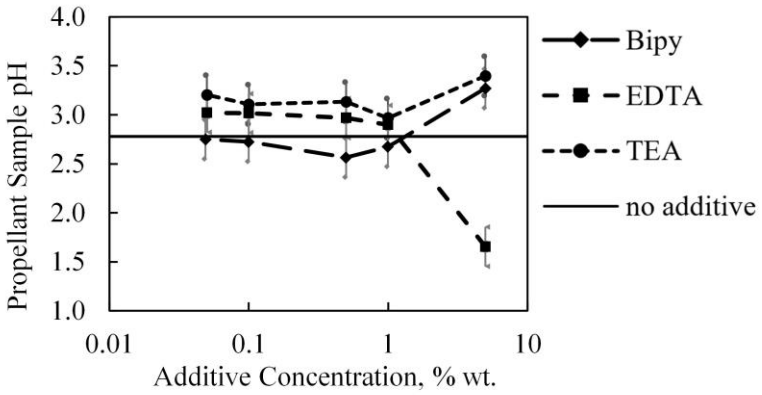

Figure 1. pH of HAN samples with chelating additives measured at room temperature.

3.3. ABSORBANCE

Neat Bipy does not absorb visible light and is colorless. When trace metals are present and Bipy forms complexes with those metals, the solution is known to absorb light in the visible spectrum [28]. Specifically, metal complexes make the solution become translucent pink or red in color. Therefore, if a solution changes color to absorb light in the visible spectrum after Bipy is added, we assume there are metal complexes with Bipy formed in the solution. We used a Varian Cary 5G spectrophotometer to measure the absorption spectrum of a 1% wt. Bipy in

water, a 1% wt. Bipy in 90% HAN sample, and a 90% HAN sample without any additive. Absorption results are shown in Figure 2.

Absorbance is the logarithm of the ratio of incident light intensity to the intensity of light transmitted through a sample with analyte according to Beer's Law. In the absorption spectra measured, a zero/baseline correction to transmission was used. Deionized water was used for the 100% transmission baseline and a cuvette stuffed with black felt was used for the 0% transmission baseline. Polystyrene cuvettes of 1 cm square internal cross-section were used in all cases. Figure 2 shows absorbance results in the visible spectrum between 400 and 800 nm wavelength. Nitrate (NO_3^-) ions absorb light in the UV spectrum, between 200 and 400 nm [30]. Nitrate ions are present in samples containing dissolved HAN. Therefore, the no-additive and 1% Bipy samples' absorbance spectra sit on the shoulder of a nitrate ion absorbance peak in the UV range while the 1% Bipy in water sample does not. Away from near ultraviolet wavelengths, between 450 and 600 nm, is a compound absorbance peak that is observed in the aqueous HAN sample with added Bipy, but not observed for the no additive or the 1% Bipy in water sample. The observed compound absorbance peak appears to consist of 2 component peaks at approximately 495 and 523 nm. This peak indicates the formation of a complex with Bipy.

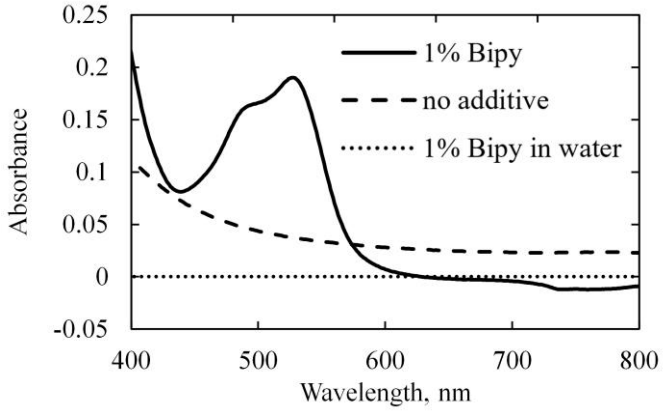

Figure 2. Absorption spectrum of 1% wt. Bipy in 90%wt. aqueous HAN compared to no additive.

We further investigate the complex evidenced in Figure 2 by dissolving iron and copper powders in nitric acid in concentrations of 6.4e-4M, which roughly corresponds to 100ppm. Bipy additive was added in concentrations corresponding to 1, 2, 3, and 10 times the molar concentration of iron or copper. 3 M Nitric acid was then diluted to achieve the desired volume and concentration of additive and then titrated onto the metal and Bipy until the metal and Bipy dissolved, and the final sample pH was 2.7±0.2pH. This is the average pH measured for Bipy in HAN samples with 1% Bipy or less as shown in Figure 1. Since the pH of Bipy and HAN solutions are the same as those with Bipy and nitric acid, differences in absorption can be attributed to constituent concentrations and not the pH-dependent stability of Bipy complexes.

The absorption spectra of Bipy+Cu samples are shown in Figure 3a, and the absorption spectra of Bipy+Fe samples are shown in Figure 3b. Complexes of Bipy with copper are observed to be a very pale blue, shown in Figure 14, reflected by the relatively low absorbance values. This blue color is due to visible light being absorbed between 600 and 800 nm with a peak between 730 and 740 nm. The location of this peak absorbance appears to fluctuate with increasing ratio of Bipy:Cu; however, this change cannot be resolved well because of a theoretical error of 2 nm. Complexes of Bipy and iron are red in color, shown in Figure 15. The color is a deeper red approaching scarlet compared with the paler color of Bipy in HAN, shown in Figure 16. This is also shown by higher Bipy:Fe absorbance values of 1-4, while the peak absorbance observed in HAN with 1% wt. Bipy was 0.2. Bipy and iron complexes absorb virtually no light above 600 nm wavelength and produce a compound peak at 523 nm and 495 nm. The sample that produced the highest peak absorbance was the 2:1 Bipy:Fe, showing that there is a nonlinear dependence of absorbance on the molar ratio of Bipy to iron. This nonlinear dependence is visible to the naked eye in Figure 15. This nonlinear absorption may be because of

an intermediate complex of iron with two Bipy molecules having a higher absorptivity than a complex of iron with one or three Bipy molecules.

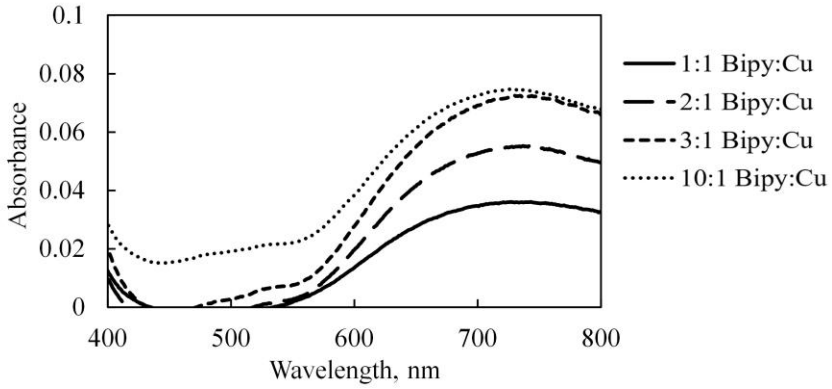

(a)

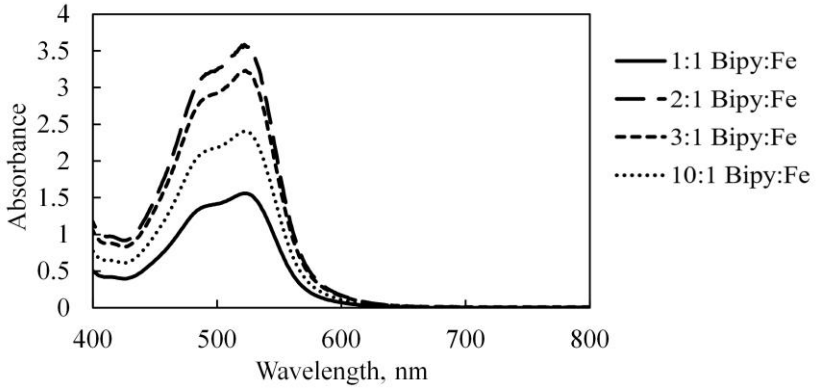

(b)

Figure 3. Absorption spectra of (a) Bipy:Cu and (b) Bipy:Fe samples of different mole ratios in nitric acid.

3.4. ISOTHERMAL TGA

Isothermal TGA at 348 K is performed to directly measure the mass loss rate over 48 hours. A sample of 30 mg is put in the TGA with the following procedure: Heat at 10 K/min to 348 K, then remain at 348 K for 48 hours. This is done under inert Nitrogen gas flowing over the sample at 60 mL/min. TGA results for no additive and 1% additive samples are shown in Figure 4. These results show that first there is a relatively fast loss of 10% of the mass, corresponding to the samples' water content. It is therefore likely that this step indicates that the water content in

the propellant sample evaporates over the first 90 minutes of the test. Following this step is a much more gradual mass loss that continues in nearly linear fashion for the remainder of the test. This corresponds to the decomposition of HAN. Starting at the 5-hour mark, to exclude the water evaporation and the startup of HAN mass loss, the last 43 hours of data are fit to a line using linear regression. The slope of this line is the linear mass loss rate. The linear mass loss rate for HAN and the coefficient of determination (R-squared value) of each linear fit are calculated, showing that each decomposition event is very close to linear with R-squared value deviating by no more than 0.0029 from unity. The linear mass loss fit parameters are given in Table 2.

For a representative 30 mg sample, the error in mass measurement corresponds to 3.3e-4 %wt. With a 10 second sampling rate, the error in mass loss rate is 3.8e-4 %/hr. A 0.026 %/hr decrease in the mass loss rate from the sample without additive was observed with the Bipy, indicating that decomposition pathways leading to gas generation are inhibited. The sample with TEA performed only slightly better than HAN without additive, at a 0.005 %/hr slower rate, and the EDTA sample decomposed 0.017 %/hr faster. 48-hour TGA tests are long and costly so only samples with 1%wt. of additive were evaluated and were chosen because they have the maximum concentration of additive without the significant pH change observed in the 5%wt. samples.

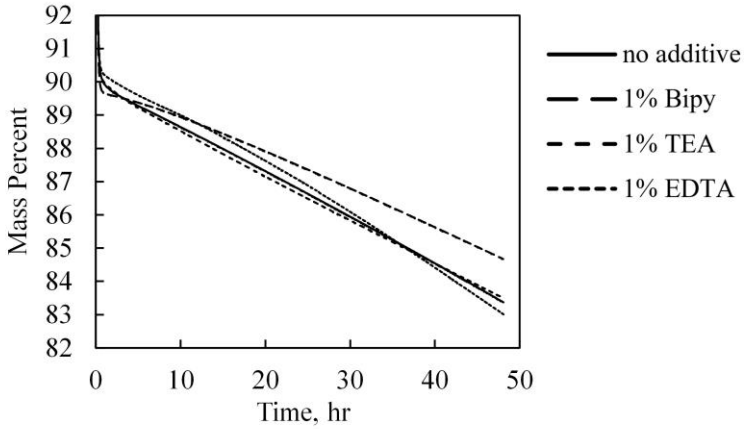

Figure 4. Isothermal TGA data for 90% aqueous HAN with and without additives in 1% concentrations.

Table 2. 348 K Isothermal TGA test parameters and linear fit results for 1% additive samples.

Sample	Initial Mass, mg	Mass Loss Rate, %/hr	Change in Mass Loss Rate, %	R-squared
No additive	33.28	0.137	0%	0.9997
1% Bipy	30.10	0.111	-20.4%	0.9988
1% TEA	31.27	0.132	-3.65%	0.9998
1% EDTA	29.18	0.154	12.4%	0.9971

3.5. DYNAMIC TGA

Heating across the decomposition temperature of HAN results in a rapid decomposition to gas that can be measured as mass loss. Dynamic TGA refers to a non-constant temperature achieved by controlled heating of the sample. In this study, a series of constant heating ramps at 2, 5, 10, 15, and 20 K/min were performed on 90% HAN and with each concentration of Bipy, TEA, and EDTA additive. The mass response to these temperature ramps is used to calculate the decomposition onset temperature and single-step Arrhenius reaction rates.

A sample dynamic ramp TGA curve of a 10 K/min heating ramp on a sample of 90% aqueous HAN without additive is shown in Figure 5. Since the heating rate is constant, there is a constant conversion between test time and temperature. Therefore, the temperature measurement can be plotted on the x-axis to produce a single-valued mass percent as a function of

temperature. Due to the same linear relationship between temperature and test time, the mass loss rate can be found as the derivative of mass with respect to temperature. At temperatures under 380 K, the mass loss corresponds to water evaporation because the mass decrease of about 10% corresponds to the known water content. HAN is known to be very hygroscopic, so it is likely that there is still some water present in the sample keeping the sample from completely drying and crystallizing [4] [31]. Nevertheless, HAN samples persist as homogeneous liquid after the evaporation of water since its melting point is at about 44°C [31] [32]. Although HAN samples persist as liquid, after most of the water evaporates they are a molten salt. Due to water evaporation during a TGA test, the same thermogram may also be used to estimate the water content of each HAN sample, as discussed in more detail in Appendix B. After water evaporation, there is a temperature range where the mass stabilizes briefly (380 – 420 K), but does not completely stop decreasing before the rapid mass loss event due to HAN decomposition at 450 K. Following this there is some unburned propellant residue that does not decompose faster than the heating rate, but does decompose by the time the sample is heated to about 520 K.

The decomposition onset temperature is found by locating the intersection of the tangent lines for the minimum mass loss rate and maximum mass loss rate immediately before and during the decomposition event. While the sample is in the stable region of slow mass loss (380 – 420 K), the rate of mass loss is not zero. In Figure 5, the black dotted curve is the derivative of the mass percent with respect to temperature, equal to the mass loss rate. The blue and red dashed lines are the tangent lines at the minimum and maximum mass loss rates during the HAN decomposition event, respectively. In Figure 5, the minimum mass loss rate is 0.0416%/K, and the maximum mass loss rate is 22.30%/K. This maximum rate is a calculated instantaneous value between two measurements; the mass loss rate shown in Figure 5 is smoothed. On the

thermogram shown in Figure 5, the minimum mass loss rate occurs at 402.3 K and the maximum is at 455.9 K. The intersection of these tangent lines in Figure 5 is located at 452.9 K, and this is the decomposition onset temperature for the 10 K/min thermogram of Figure 5.

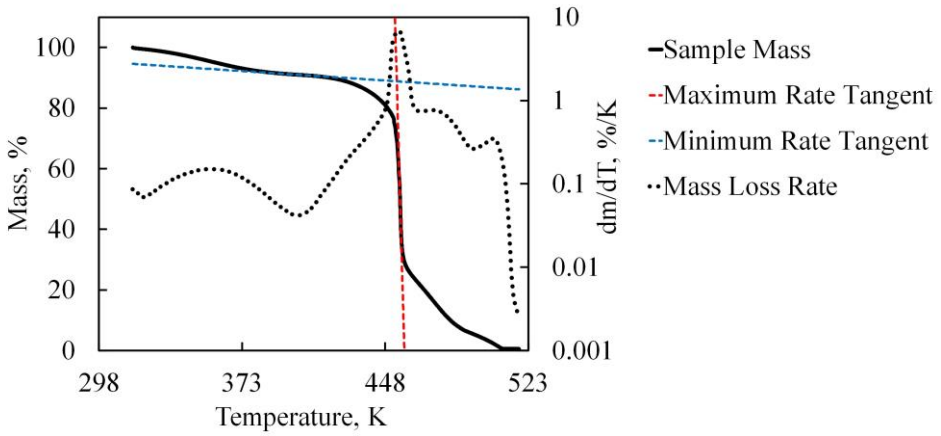

Figure 5. A dynamic TGA thermogram of a 10 K/min constant heating ramp applied to 90% aqueous HAN with tangent lines at maximum and minimum mass loss rate about the HAN decomposition event showing the location of the decomposition onset temperature at 452.9 K.

The decomposition of each HAN and additive sample is measured by TGA at 2, 5, 10, 15, 20 K/min constant heating rates, and the decomposition onset temperature calculated. Results are shown in Figure 6. The no additive data are shown in Figure 6d as decomposition onset temperature versus heating rate. As shown in Figure 6d, above a 10 K/min heating rate, the decomposition onset temperature of HAN with no additive begins to plateau at about 454.8 K. For onset temperatures, the plateau region found using HAN without additive can be compared with the same high heating rate tests using HAN with additive since the heating rate is no longer dominating the decomposition onset measurement. The average decomposition onset temperature of the 10, 15, and 20 K/min heating rate points for Bipy, TEA, and EDTA are 461.8, 453.9, and 461.3 K respectively.

As shown in Figure 6, the decomposition temperatures do not show a simple proportionality with the range of additive concentrations measured. More additive does not

necessarily mean that the decomposition temperature increases. The experimental variation is high, while the measurement error on temperature is very low at 0.1 K. This means that there is experimental or calculation error causing fluctuation of the measured decomposition onset temperature that is not related to the quantity of additive. The range between the lowest and highest decomposition onset temperature of each heating rate series is used as a measure of variation or consistency within each series. The fluctuations observed in onset temperature are discussed in greater detail in section 4.2. Considering only heating rates above 10 K/min, the average onset temperature range for each additive is 5.2, 23.1, and 30.6 K for Bipy, TEA, and EDTA respectively. This means that the decomposition onset temperatures observed for samples with Bipy are within a smaller range of temperatures than those for TEA and EDTA.

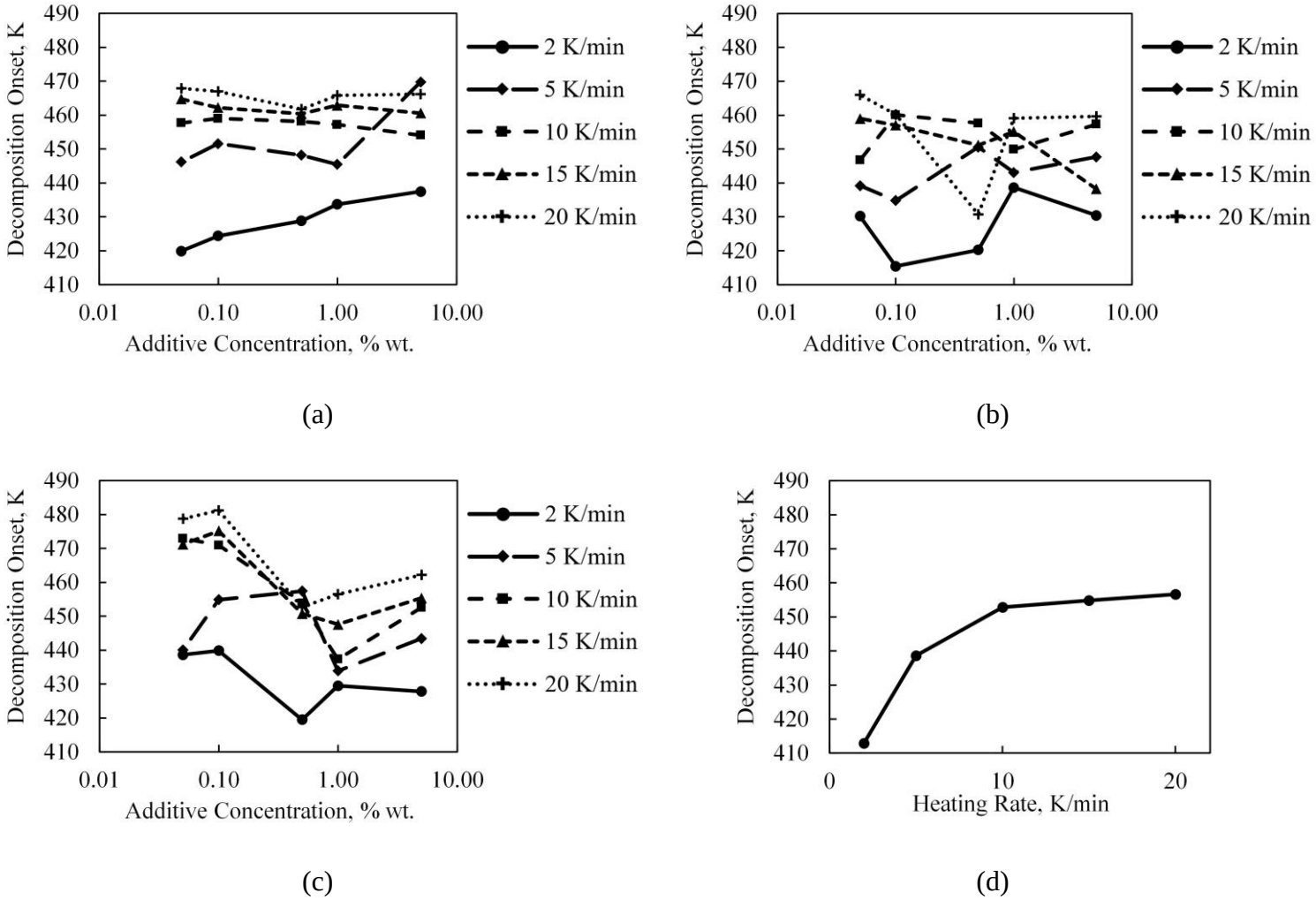

Figure 6. Decomposition onset temperatures of 90% HAN with and without additives: (a) Bipy; (b) TEA; (c) EDTA; (d) 90% aqueous HAN without additive.

CHAPTER 4: DISCUSSION

4.1. COMPARING ISOTHERMAL RESULTS WITH PH

Results for isothermal decomposition at 348 K of 1% additive samples compared with the no additive sample show that while bipy can inhibit HAN decomposition, TEA has a significantly lesser inhibitive effect and EDTA can even catalyze decomposition. These results show that a mechanism based on H^+ alone does not adequately explain the inhibitive effect of Bipy on HAN decomposition. After 48 hours, the sample with 1% Bipy has 1.3% more mass remaining than the HAN sample with no additive. Although this is a small difference, it is significant since the TGA measurement error is sensitive to 0.00033% of the 30 mg sample. The TEA sample has just 0.13% more mass remaining than the sample with no additive and the EDTA sample ends the 48-hour test with 0.36% less mass than the sample with no additive. These results show that Bipy and TEA have inhibited the decomposition of HAN at 348 K.

1% Bipy provided 5 times the inhibition to isothermal mass loss rate of HAN compared to the inhibition from 1% TEA, suggesting that changing the pH is not the only mechanism by which Bipy and TEA affect HAN decomposition.

Acid dissociation constants of the protonated form of the chosen additives are given in Table 3 for the dissociation of each chelating agent into H^+ and its conjugate base. EDTA can be written as H_4EDTA to note the hydrogens in the acetic acid groups that would be the first to dissociate. These notations refer to the same molecule.

The acid dissociation constants (pK_a) of protonated Bipy and TEA are both higher than the 2.8 equilibrium pH of 90% aqueous HAN, so these species are not expected to release additional H^+ ions when dissolved in solution. Instead they are able to bond with free H^+ ions,

recombining into their protonated form. Protonated EDTA has two acid dissociations with a pK_a less than the pH of the HAN solution, therefore EDTA is expected to release two H^+ per molecule. Releasing additional H^+ catalyzes HAN decomposition, overshadowing any metal sequestration properties. The effect of acid dissociation is observed in the pH measurements of HAN solutions with 5% wt. additive concentrations in Figure 1. Figure 1 shows that acid dissociation of higher concentrations of each additive changes the sample to a lower pH for EDTA and a higher pH for Bipy and TEA.

The pH of samples tested are measured and compared with data at 298 K and 1 atm. This is the relevant regime for the formation of chelate complexes in HAN solutions before their use, but pH and pK_a properties of samples may change based on the elevated temperatures and decreased water content during TGA testing. For example, with less water in the mixture and at elevated temperature, the pH is expected to decrease. In theory this could change whether the additives dissociate or recombine with free H^+ ions. However, the isothermal decomposition rates reflect the comparison of pH and pK_a values at room temperature so while the actual values may change their comparison remains valid. The same logic applies to the stability of each chelate complex, and particularly Bipy. If the stability of Bipy complexes were compromised by the elevated temperature and decreased pH, then no decomposition inhibition should be observed past that expected by its acid recombination.

If H^+-based mechanisms are the only way that these additives affect the decomposition of HAN, then TEA should have the best inhibition properties because it has the highest pKa. Therefore, pH does not adequately explain why Bipy had five times the inhibitive effect on HAN isothermal mass loss rate. Spectrophotometry results indicate that sequestration of iron by Bipy is a possible explanation for its relative effectiveness.

Table 3. Acid dissociation constants of selected ligand species at 298 K [33] [34] [35].

Additive Species	pK_a
Bipy(H^+)	4.4
TEA(H^+)	7.74
H_4EDTA	2
H_3EDTA^-	2.7

4.2. DECOMPOSITION ONSET TEMPERATURES

Like the results for isothermal mass loss rate, the results for decomposition onset temperatures show that Bipy, TEA, and EDTA affect the decomposition of HAN differently. Bipy samples show a 7.0 K increase in the decomposition onset temperature compared with no additive, while TEA and EDTA samples do not show a clear change. Additionally, none of the samples showed a significant dependence of decomposition onset temperature on the additive concentration in the range investigated. The method of calculating decomposition onset temperature is heavily dependent on the maximum mass loss rate and is more easily influenced by procedural error, obscuring meaningful results from the TEA and EDTA data.

The maximum mass loss rate is sensitive to small changes in the shape of the mass loss curve. If an error occurs that affect this small section of the TGA curve, the decomposition onset temperature calculated from the TGA curve can change significantly. When the sample reacts endothermically, the TGA thermogram can double back on itself as the measurement thermocouple briefly measures a lower temperature. This can rapidly flip the sign of the derivative making the determination of the maximum mass loss rate less clear. These are consequences of HAN decomposing quickly, losing the bulk of its liquid mass in seconds, and thereby amplifying random errors to large variations in decomposition onset temperature.

Decomposition onset temperatures for HAN start to plateau at and above 10 K/min. This is because the heating rate becomes faster than the thermal diffusion and bulk heating of the sample such that the decomposition starts at its maximum rate and temperature each time. To minimize the influence of the heating rate, decomposition onset temperatures acquired at or above 10 K/min heating rate are compared in Figure 7. According to the decomposition onset temperature data, Bipy samples produce a consistently higher decomposition temperature than HAN without any additive. Figure 7 shows the average and range of onset temperatures measured with and without additives visually for the data above 10 K/min heating rate. Above 10K/min, the average onset temperature for Bipy is 461.8 K, while for HAN without any additive it is 454.8 K. The 7.0 K difference between these decomposition onset temperature averages is larger than the range for both Bipy-added and HAN onset temperatures, making it a significant difference.

Unlike the low range of 5.2 K observed for Bipy sample onset temperature series, the high ranges of 23.1 and 30.6 K for TEA and EDTA eclipse the differences observed between these samples and the no additive samples. Therefore, the only conclusion that can be made from the TEA and EDTA series is that the decomposition onset temperature is more unstable for samples containing these additives compared to samples containing Bipy or no additive. Despite any error, samples containing Bipy or no additive exhibited a smaller range of decomposition onset temperatures, leading to the conclusion that Bipy inhibited the decomposition of HAN.

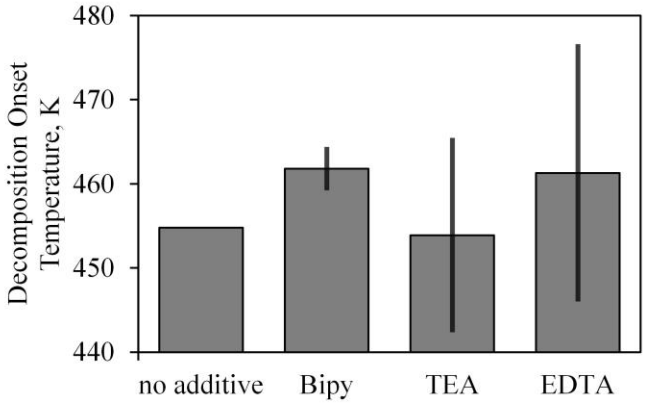

Figure 7. Bar graph comparing decomposition onset temperature averages and ranges for data above 10 K/min heating rate.

4.3. REACTION RATE PARAMETERS AND KINETIC COMPENSATION

Reaction rate parameters are calculated as an additional method for examining the influence of additives on the reaction rate. These rate parameters follow a proportional trend established in literature, thought to be due to the Kinetic Compensation Effect (KCE) [36] [37]. Since the rate parameters agree with those from literature, it shows that the reaction phenomena – the decomposition of HAN – observed by TGA methodology in this study are the same as those observed in literature [38].

Reaction rate parameters are theoretically independent of heating rate and give an estimate of the rate of the reaction itself, under a couple of assumptions. In this work, first order Arrhenius reaction rate parameters are fit from experimental TGA data using the Ozawa/Flynn/Wall (OFW) method [39] [40] [41]. The first order reaction rate formulation is

$$k = Aexp(\frac{-E_a}{RT}), \quad (1)$$

where for any reaction of rate k, A is the pre-exponential frequency factor, T is the temperature, R is the universal gas constant, and E_a is the activation energy in the same units as

RT. A and k have units of s^{-1}, while the E_a/RT is a unitless fraction of molecules with threshold energy E_a available.

Reactions observed by TGA are analyzed by a nondimensional fraction of sample reacted (α), equivalent to the mass percent change over a single step, where its rate of change is proportional to the reaction rate and a function of α:

$$\frac{d\alpha}{dt} = k(T)f(\alpha). \quad (2)$$

For a TGA test of constant heating rate $\beta \equiv dT/dt$, equation 2 can be written as:

$$\frac{d\alpha}{dt} = \beta\frac{d\alpha}{dT} = Aexp(\frac{-E_a}{RT})f(\alpha). \quad (3)$$

Solving for alpha by integrating

$$\int_{\alpha_0}^{\alpha}\frac{d\alpha}{f(\alpha)} = \int_{T_0}^{T}\frac{A}{\beta}exp(\frac{-E_a}{RT})dT, \quad (4)$$

from a point (T_0, α_0) before the reaction to a chosen conversion point during the reaction (T, α), cannot be done analytically but has been solved numerically in a variety of ways. The OFW method uses the Doyle approximation for the temperature integral [39] [40] [42] [43]. In this work, $f(\alpha) = 1 - \alpha$ is used in accordance with the ASTM E1641-16 standard and the TA Instruments recommendation [42] [41]. This choice of $f(\alpha)$ assumes that the reaction is a single-step, global reaction, providing accurate results for complex decompositions when there is a single rate-limiting mechanism [43]. This is a reasonable approximation for HAN since its autocatalysis has been found to be mainly dependent on solution acidity and thereby proton transfer to hydroxylamine [6]. The objective of this study is to determine the effect of additives on the onset of the decomposition and not to accurately determine the reaction rate, thus, a conversion point of $\alpha = 0.05$ was used for this study.

Armed with a conversion point and an approximate solution for the temperature integral in equation (4, the activation energy E_a and the pre-exponential A can be solved for using linear regression. Taking the natural logarithm of equation 3 makes the linear nature clear, producing

$$\log(\beta) = \frac{-E_a}{RT} + \log\left(\frac{Af(\alpha)}{d\alpha/dT}\right), \quad (5)$$

which is a linear equation of $\log(\beta)$ vs. $1/T$ where the slope is proportional to the activation energy and the y-intercept is related to the pre-exponential by the temperature integral. The Doyle integral approximation is solved by the recommended iterative method to increase the accuracy of the approximation [42] [41] [43].

The conversion point of $\alpha = 0.05$ corresponds to 5% of the HAN mass lost as the decomposition step is assumed to be only due to global HAN decomposition. For a 1% additive sample the conversion point is

$$W_C = (100\% - W_A)W_{HAN}(1 - \alpha) + W_A, \quad (6)$$

where W_C is the percent of total sample weight at the conversion point (T, α), W_A is the weight percent of additive added to the sample, α is the fraction of sample reacted, and W_{HAN} is the percent weight of HAN in the pre-additive solution. In this work, $\alpha = 0.05$ and $W_{HAN} = 90\%$. Equation (6 assumes that all water and only water has evaporated and that none of the additive has decomposed.

Constant heating rate dynamic TGA thermograms at rates of 2, 5, 10, 15, and 20 K/min of 90% aqueous HAN without additive ($W_A = 0\%$) are shown in Figure 8, with the conversion point for calculating Arrhenius parameters at $W_C = 85.50\%$ marked by a horizontal line. As intended, the conversion point falls 5% into the beginning of the main HAN mass loss event, well after the initial water evaporation mass loss event and just before most of the HAN

decomposes. Like decomposition onset temperature, the temperature at the conversion point is higher for a higher heating rate.

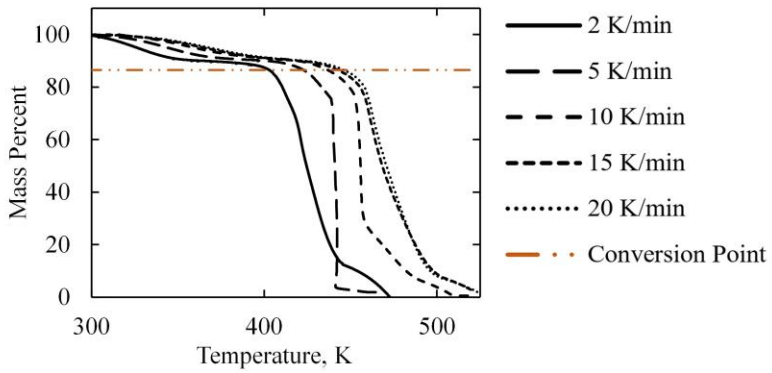

Figure 8. Constant heating rate dynamic TGA thermograms of 90% aqueous HAN with the conversion point for calculation of Arrhenius parameters shown.

The temperature at which the conversion point percent weight for each heating rate occurs is converted to Kelvin and inverted to produce the Arrhenius plot of log heating rate vs. inverse temperature, shown in Figure 9. The linear fit shown on the plot has slope -9344.9 K^2/min and y-intercept 23.816 K/min. This fit generates a coefficient of determination (R-squared) of 0.987, showing that although imperfect, the linear fit is adequate for the onset region of HAN decomposition where α is low.

Conversion points and heating rates from TGA thermograms at rates of 2, 5, 10, 15, and 20 K/min of 90% aqueous HAN without additive are used to produce a sample Arrhenius plot of log heating rate vs. inverse temperature, shown in Figure 9. The linear fit shown on the plot is for a no additive sample and has slope -9344.9 K^2/min and y-intercept 23.816 K/min. This fit generates a coefficient of determination (R-squared) of 0.987, showing that although imperfect, the linear fit appears acceptable for the onset region of HAN decomposition where α is low. For the data in Figure 9, the activation energy and pre-exponential factor are found to be 171.5±11.4 kJ/mol and 40.2±1.2 s^{-1}.

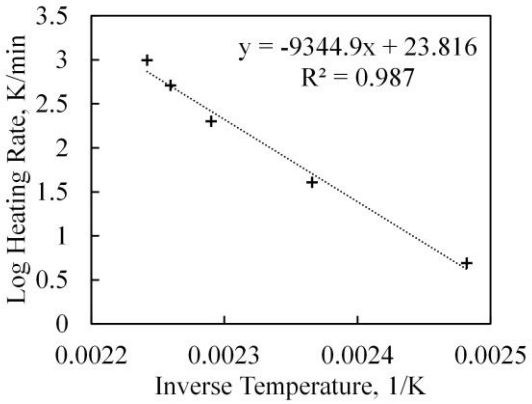

Figure 9. Arrhenius plot of log heating rate vs. inverse temperature for of 90% aqueous HAN sample with linear fit shown.

The activation energy and pre-exponential parameters can then be found by iterating through the parameters from the Doyle integration approximation, a and b, using

$$E_a = \frac{R}{b}\frac{\Delta \log(\beta)}{\Delta(1/T)}, \tag{7}$$

iterating on b, and then calculating

$$A = \frac{-\beta R}{E_a}\log(1-\alpha)10^a \tag{8}$$

using the value of a corresponding with the final b value. a and b parameters can be found tabulated in [42] [41]. The error in activation energy is calculated from the uncertainty in the slope calculated by linear regression with the fit shown in Figure 9 as recommended by the ASTM E1641-16 standard [42]:

$$\delta E_a = E_a\frac{\delta m}{m} = \frac{E_a}{m}\left[\frac{n\sum(\delta y_i)^2}{(n-2)[n\sum x_i{}^2-(\sum x_i)^2]}\right]^{1/2}. \tag{9}$$

δE_a is the uncertainty in activation energy, m is the slope calculated using linear regression, and δm is the uncertainty associated with that slope. In equation 9, n is the number of (x_i, y_i) pairs, corresponding to each $(1/T, \log(\beta))$ pair when calculating activation energy. $\delta y_i = y_i - (mx_i + b)$ is the uncertainty in an individual value of y_i, the vertical distance between it and the linear fit.

For each HAN sample, the calculated first-order activation energy and frequency factor for each propellant sample are plotted in Figure 10. In Figure 10 the horizontal line represents the HAN sample without additive. The samples with additive have a higher activation energy. Higher activation energy indicates in theory that the decomposition for those samples is inhibited. This may not be true due to kinetic compensation. Specifically, since the chosen conversion point (the value of α) is 0.05, this reaction rate is the rate for the first 5% of the sample to decompose. The vertical bars represent the linear regression error associated with the fit of the reaction rate parameters. As predicted by the KCE, the trends in the activation energy results appear very similar to the results for frequency factor.

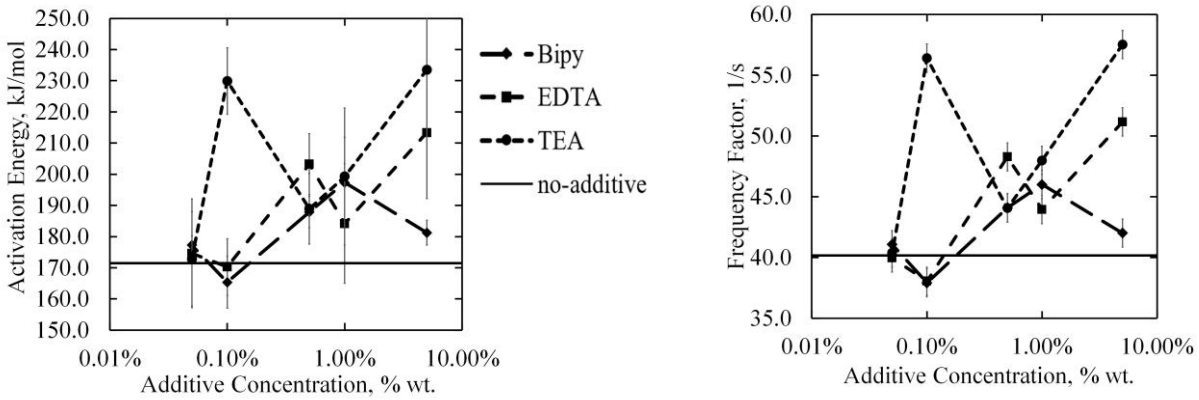

(a) (b)

Figure 10. Parameters for the Arrhenius reaction rate calculated from dynamic TGA using Ozawa/Flynn/Wall method. (a) Activation energy in kJ/mol with error; (b) Natural logarithm of Frequency factor/ pre-exponential in s^{-1} parameter with error.

Computational and experimental work elucidates the mechanisms of HAN decomposition and calculate the rate constants of each [6]. Some of the rate constant parameters for HAN from literature are shown in Figure 11, compared with those calculated in this work. A positive, linear correlation between frequency factor and activation energy is clear. This is an observation of the KCE, which states that the frequency factor is a result of the Arrhenius rate equation formalism [36] [37]. When a procedural change is made that changes the activation energy, a frequency factor is calculated that abides by the linear compensation law,

$$\log(A) = \frac{E_a}{R\theta} + \lambda, \tag{10}$$

where θ and λ are linear fit coefficients. This linear relationship is an implicit assumption in numerically fitting experimental data to the Arrhenius rate equation. Activation energy and the frequency factor are fundamentally coupled for complex reaction phenomena that include many steps and intermediate species such that the physical description of 'frequency factor' is dubious at best. The linear fit parameters λ and θ in equation 10 for the data collected by Zhang are -3.497 s^{-1} and 446.3 K respectively [6]. For the data from this work, λ and θ are -9.887 s^{-1} and 418.2 K.

The parameters from this work neatly create a linear kinetic compensation trend and exhibit consistency with rate parameters measured in other work. The parameters calculated in this work are each at a higher activation energy and frequency factor, except for the outlier from Kondkrikov's work. This is expected as the final value of the rate parameters are highly dependent on sample and experimental conditions as discussed by Brill et al. [38]. The reason for the differing range of reaction rate parameters may also be dependent on the conversion point used for calculating the parameters or the method itself. Using a conversion point of $\alpha = 0.05$ effectively ignores the decomposition of the last 95% of the mass. This works around the issue in

decomposition onset temperature calculation of depending on the maximum mass loss rate, however, the calculation of reaction rate parameters presents its own inaccuracies.

Due to the similar magnitudes and frequency factor versus activation energy trend, there is considerable overlap of the reaction phenomena being observed. It should be no surprise that a complex physical phenomenon such as the decomposition of HAN is inadequately described by an equation with two variational parameters. Nevertheless, fitting Arrhenius reaction rate parameters with a repeatable degree of kinetic compensation as shown by the agreement between many studies in Figure 11 indicates that the same reaction phenomena are being observed [38].

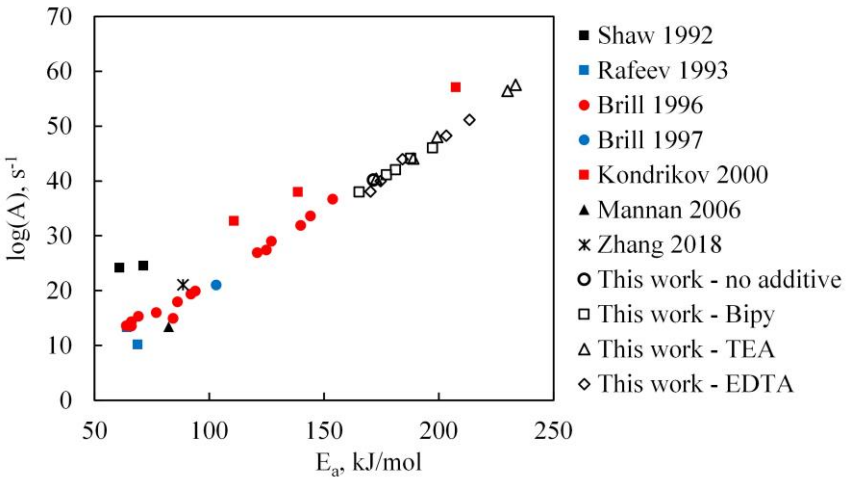

Figure 11. Literature review by Zhang [6] comparing Arrhenius parameters of various HAN samples with their analytical prediction. No additive (90% aqueous) HAN, Bipy, TEA, and EDTA additive data from this work are compared.

4.4. REACTION RATE INHIBITION

Even though the frequency factor and activation energy parameters are coupled, the reaction rate calculated at 348 K appears to be inhibited. However, the series for each additive show similar variation and similar trend. Due to the similarity of reaction rate results for each additive, the inhibitive or catalytic effects of the additives tested are found to be too small to be captured by the OFW method of determining reaction rate parameters. This indicates that

although Bipy, TEA, and EDTA were observed to affect the decomposition of HAN according to results from isothermal TGA and onset temperature calculations, they do not significantly change its rate-limiting mechanism. The differences calculated in reaction rate must be artefacts of the measurement and post-processing procedure.

In Figure 12, the data from Figure 10 is used to calculate reaction rates using a temperature of 348 K, the same temperature used in isothermal tests. The reaction rate parameters as shown in Figure 10 are clearly coupled to each other due to the KCE. Despite this coupling, the kinetic reaction rate exhibits a decreasing trend with increasing additive concentration to a lower reaction rate than measured for no additive samples. However, the series for each additive produces similar decreasing trends each with similar variance. This is in contrast with the isothermal decomposition and onset temperature data where Bipy showed inhibitive effect while TEA and EDTA showed a catalytic or no significant effect. Therefore, the decreasing of the kinetic rate calculated at 348 K is due to error from inaccurate assumptions in the application of the OFW method.

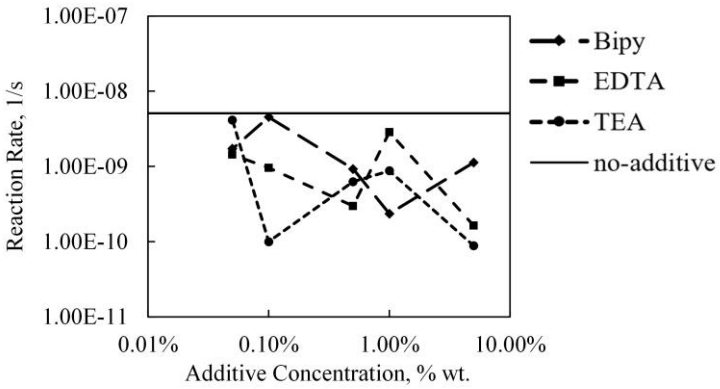

Figure 12. Arrhenius reaction rates calculated using the data in Figure 10 and a temperature of 348 K.

Independent of the reported error from linear regression on the Arrhenius plot, there is additional error in the assumptions of a first order reaction rate, Doyle's integral approximation,

and using a linear conversion function. Approximating HAN decomposition as a single step, first order reaction should be reasonable for HAN since its autocatalysis has been found to be mainly dependent on proton transfer to hydroxylamine [6]. The proposed mechanism by which chelating additives are proposed to inhibit HAN decomposition is not the primary acid catalyzed mechanism. This is confirmed by the lack of serious change in the reaction rates that should correspond to the isothermal TGA results.

Alternative methods for solving the Arrhenius equation and fitting reaction rates using alternate temperature integral solution methods or alternate conversion functions are discussed by Vyazovkin et al. [43]. The method used in this work was used for its simplicity, but other methods of approximating kinetic models might better capture the secondary nature of the effect of chelating agents compared to the primary proton transfer mechanism. Particularly, methods that use longer time scales such as combining multiple isothermal measurements to calculate rate parameters might produce better results. Hansen observed that some chelating agent additives extended the lifetime of HAN samples observed over multiple weeks [3]. It stands to reason that the secondary effect of chelating agents becomes more pronounced at lower temperature and pressure conditions and on longer time scales where the secondary metal-catalyzed mechanism has time to compete with the primary acid-catalyzed decomposition mechanism.

4.5. BIPY COMPLEX ABSORBANCE AND SPECIATION

Absorption peaks found in results from visible spectrum spectrophotometry confirm that the aqueous HAN contains metal ions in trace quantities and that Bipy forms chelate complexes with them.

The absorbance peak located at 527 nm in Figure 2 corresponds with the expected peak absorbance for $[Fe(bipy)_3]^{2+}$ at 522 nm, allowing for a slight redshift [28]. The peak absorbance for $[Fe(bipy)_3]^{3+}$ is at 610 nm which is outside the measured absorbance signal due to iron,

therefore all measured complexes are assumed to be $[Fe(bipy)_3]^{2+}$ [28]. The relative intensity of this peak can be used to estimate the iron concentration. According to the Beer-Lambert law, the fractional intensity of light that is absorbed by a molecule in solution is proportional to the concentration of that molecule in the solution. To 1st order, the Beer-Lambert law is

$$Abs = \log_{10}\left(\frac{I_{100\%}-I_{0\%}}{I-I_{0\%}}\right) = \epsilon lc, \tag{11}$$

where Abs is the absorbance of a particular wavelength of light, measured by the decadic logarithm of the ratio of light transmitted through the reference to the intensity of light transmitted through the sample. In the absorption spectrum of the 1% Bipy sample in Figure 2 there is a concentration of Bipy four orders of magnitude greater than the expected concentration of iron, therefore only saturated Bipy:Fe complexes with three Bipy molecules are expected to be present. Schilt gives molar absorptivity for $[Fe(bipy)_3]^{2+}$ and $[Fe(bipy)_3]^{3+}$as 8650 and 330 M^{-1} cm^{-1} respectively [28]. Using the absorptivity of $[Fe(bipy)_3]^{2+}$ along with the measured peak absorbance at 527 nm, a concentration of 1.2 ppm Fe is found. This corresponds well with the 0.9 ppm measured with ICP-MS (Table 1) and further confirms the existence of trace metal impurities including iron. It also indicates that iron ions are sequestered by Bipy at the equilibrium pH of HAN.

The wavelength of light absorbed corresponds to physical properties of the complex that absorbs the light. This means that complexes of different metal ions with different sizes absorb different wavelengths of light and that each individual absorbance peak corresponds with either a complex of a different metal species or a complex with different numbers of Bipy. For example, a different wavelength may be observed for the complexes with ratios of 2:1 Bipy:Fe, 3:1 Bipy:Fe, and 2:1 Bipy:Cu. The absorbance peaks measured for HAN are compared with those for Fe+Bipy and Cu+Bipy solutions, all normalized to the peak absorbance shown in

Figure 13. The 3:1 Bipy:Fe ratio and 2:1 Bipy:Cu ratio spectra are presented because iron commonly has a coordination number of 6 and copper commonly has a coordination number of 4. It is therefore expected that the 3:1 and 2:1 Bipy:Fe and Bipy:Cu respectively are the most stable complexes with all the metal ion's coordination sites filled, present in a solution with excess Bipy.

The wavelength of peak absorbance for copper is 742 nm while the wavelength of the peak of Fe+Bipy and 1% Bipy-HAN are 523 nm. Furthermore, the Fe+Bipy and Bipy-HAN samples show the same secondary peak at 495 nm. The zoomed-in inset shows that there is no significant absorbance observed at 742 nm in the 1% Bipy in HAN sample. The fluctuations observed in the inset are most likely the amplification of noise by the zero/baseline correction. These results suggest that adding Bipy to a HAN solution with trace iron content causes Fe+Bipy complexes to form with no noticeable copper complexes. This suggests that the effect on decomposition rate and activation energy observed due to Bipy is because of chelation and sequestration of iron.

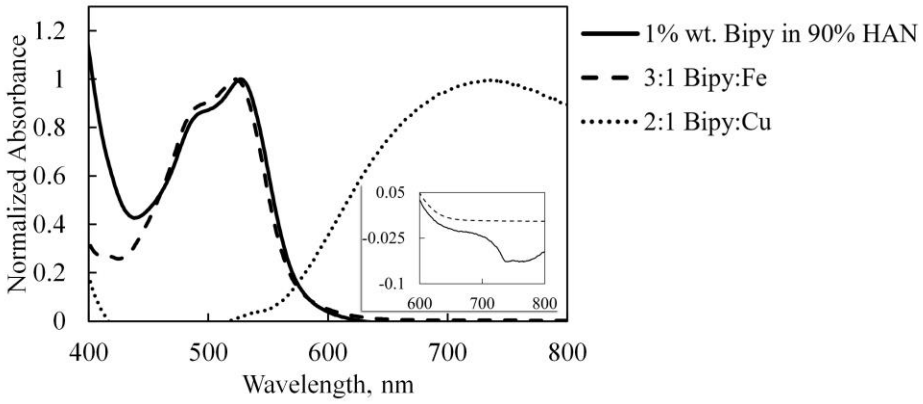

Figure 13. Comparison of absorbance spectra of 1% wt. Bipy in 90% HAN to samples of Bipy+Fe and Bipy+Cu in nitric acid solution, normalized to the peak absorbance for comparison of peak wavelength values.

CHAPTER 5: CONCLUSION

HAN samples using 90%wt. aqueous HAN as solvent were made with and without chelating agent additive. Using data obtainable by the same TGA machine, multiple methods of analysis were performed on these samples. Methods included isothermal TGA and dynamic TGA using multiple constant heating rates, which allowed for the calculation of the isothermal decomposition rate, the decomposition onset temperature, and first order Arrhenius reaction rate parameters. 2,2'-bipyridine (Bipy), triethanolamine (TEA), and ethylenediaminetetraacetic acid (EDTA) were studied as 0.05, 0.1, 0.5, 1, and 5% by weight additives in 90% aqueous HAN by weight.

An isothermal decomposition rate of 0.137%/hr at 348 K was observed for HAN at 348 K. Addition of 1% Bipy and 1% TEA reduced the isothermal decomposition rate by 20.4% to 0.109%/hr and by 3.65% to 0.132%/hr, respectively. The addition of 1% EDTA increased the isothermal decomposition rate by 12.4% to 0.154%/hr. Isothermal results imply that there are other relevant mechanisms at play like pH-dependent complex stability and acid dissociation that mean chelating ability alone is not a good qualifier for an additive to HAN-based propellant.

Bipy was found to increase the decomposition onset temperature from 454.8 K to 461.8 K while TEA and EDTA made the decomposition onset temperature more unstable without significantly changing it. First order reaction rates calculated by the Ozawa-Flynn-Wall (OFW) method were found to be insufficient in capturing the effects of the additives tested. The reaction rates did, however, neatly fit into the positive trend of pre-exponential vs. activation energy

parameters that is due to the Kinetic Compensation Effect. This shows that the decomposition mechanism studied in this work is the same as those in other studies in the literature.

Spectrophotometric results show that Bipy forms complexes with both copper and iron in solutions at the same equilibrium pH as 90% HAN. Comparing these results with 1% Bipy added to 90% HAN shows that there are trace iron impurities on the order of 1 part per million and that they form chelate complexes with the added Bipy. Results of ICP-MS indicate that there may be other trace metal impurities present in HAN that catalyze HAN through a secondary decomposition mechanism.

Bipy, a chelating agent that forms complexes with trace quantities of iron, is found to reduce the decomposition rate of HAN, but only in the low-temperature limit, observed in this study at 348 K. Chelating agents that form stable metal complexes at low pH such as Bipy increase the storage stability by decreasing the rate of decomposition in the low temperature and long timescale limit. To effectively inhibit HAN decomposition, the additive must also have pK_a higher than 2.8 such that no acid dissociation occurs. This effect is observed even at part per million concentration of metal impurities. In the fast, high-temperature decomposition of HAN, pH plays a much greater role than the effect of complexing metal impurities. Future work should directly investigate the effect of pH neutralizing additives on HAN decomposition to find whether targeting the primary decomposition mechanism can have greater inhibitive effect in storage conditions.

REFERENCES

[1] R. K. Masse, R. A. Spores and M. Allen, "AF-M315E Advanced Green Propulsion - GPIM and Beyond," in *AIAA Propulsion and Energy 2020 Forum*, Virtual, 2020.

[2] K. Hori, T. Katsumi, S. Sawai, N. Azuma, K. Hatai and J. Nakatsuka, "HAN-based Green Propellant, SHP163 - Its R&D and Test in Space," *Propellants, Explosives, Pyrotechnics,* vol. 44, pp. 1-5, 2019.

[3] R. Hansen, E. Backof and H. J. deGreiff, "Process for Assessing the Stability of HAN-Based Liquid Propellants," European Research Office of the U.S. Army, London, England, 1989.

[4] D. G. Harlow, R. E. Felt, S. Agnew, G. S. Barney, J. M. McKibben, R. Garber and M. Lewis, "Technical Report on Hydroxylamine Nitrate," U.S. Department of Energy, 1998.

[5] H. Lee and T. A. Litzinger, "Chemical Kinetic Study of HAN Decomposition," *Combustion and Flame,* vol. 135, pp. 151-169, 2003.

[6] K. Zhang and S. T. Thynell, "Thermal Decomposition Mechanism of Aqueous Hydroxylammonium Nitrate (HAN): Molecular Simulation and Kinetic Modeling," *Journal of Physical Chemistry,* vol. 122, no. 41, pp. 8086-8100, 2018.

[7] R. Agnihotri and C. Oommen, "Cerium Oxide Based Active Catalyst for Hydroxylammonium Nitrate (HAN) Fueled Monopropellant Thrusters," *RSC Advances,* vol. 8, no. 40, pp. 22293-22302, 2018.

[8] M. J. Wainwright, J. L. Rovey, S. W. Miller, B. D. Prince and S. P. Berg, "Hydroxylammonium Nitrate Species in a Monopropellant Electrospray Plume," *Journal of Propulsion and Power,* vol. 35, no. 5, pp. 922-929, 2019.

[9] M. S. Glascock, P. D. Drew and J. L. Rovey, "Thermodynamic and Transport Properties of Hydroxylammonium Nitrate-Based Electric Solid Propellant Vapor," in *AIAA SciTech Forum*, San Diego, California, 2019.

[10] N. Rasmont, E. J. Broemmelsiek and J. L. Rovey, "Linear Burn Rate of Green Ionic Liquid Multimode Monopropellant," *Combustion and Flame,* vol. 219, pp. 212-224, 2020.

[11] T. Katsumi and K. Hori, "Successful Development of HAN Based Green Propellant," *Energetic Materials Frontiers,* 2021.

[12] E. W. Schmidt, "Hydroxylammonium Nitrate Compatibility Tests with Various Materials," U.S. Army Ballistic Research Laboratory, 1990.

[13] R. Amrousse, H. Kagawa, K. Hatai, H. Ikeda and K. Hori, "The Effect of Iron Metal Ions and Chelating Agents of Iron on the Thermal Decomposition of HAN-Based Liquid Monopropellant," in *AIAA Joint Propulsion Conference*, Orlando, 2015.

[14] C. Zhang, Thermal Decomposition Study of Hydroxylamine Nitrate During Storage and Handling, Texas A&M University, 2006.

[15] S. Hoyani, R. Patel, C. Oommen and R. Rajeev, "Thermal Stability of Hydroxylammonium Nitrate (HAN)," *Journal of Thermal Analysis and Calorimetry,* vol. 129, pp. 1083-1093, 2017.

[16] R. E. Ferguson, A. A. Esparza and E. Shafirovich, "Combustion of Aqueous HAN/Methanol Propellants at High Pressures," *Proceedings of the Combustion Institute,* 2020.

[17] S. P. Berg and J. L. Rovey, "Decomposition of Monopropellant Blends of Hydroxylammonium Nitrate and Imidazole-Based Ionic Liquid Fuels," *Journal of Propulsion and Power,* vol. 29, no. 1, pp. 125-135, 2013.

[18] S. P. Heneghan, S. Zabarnick, D. R. Ballal and W. E. Harrison III, "JP-8+100: The Development of High-Thermal-Stability Jet Fuel," *Transactions of the ASME,* vol. 118, pp. 170-179, 1996.

[19] A. M. Da Costa Ferreira and L. L. De Oliveira Duarte, "The Effect of Triethanolamine on the Iron(III)-Catalysed Decomposition of Hydrogen Peroxide," *Journal of Coordination Chemistry,* vol. 24, no. 4, pp. 339-350, 1991.

[20] C. F. Bell, Principles and Applications of Metal Chelation, Oxford: Oxford University Press, 1977.

[21] R. A. Goyer and T. W. Clarkson, "Toxic Effects of Metals," in *Casarett & Doull's Toxicology: The Basic Science of Poisons*, McGraw-Hill, 2001, pp. 811-867.

[22] W. Siegert, "Boosting the Antimicrobial Efficiency of Multifunctional Additives by Chelating Agents," *SOFW-Journal,* no. 140, 2014.

[23] J. R. Hart, "EDTA-Type Chelating Agents in Everyday Consumer Products: Some Food, Cleaning, and Photographic Applications," *Journal of Chemical Education,* vol. 62, pp. 75-76, 1985.

[24] K. Asemave, "Greener Chelators for Recovery of Metals and Other Applications," *Organic and Medicinal Chemistry,* vol. 6, no. 4, 2018.

[25] R. C. Striebich, B. Grinstead and S. Zabarnick, "Quantitation of a Metal Deactivator Additive by Derivatization and Gas Chromatography-Mass Spectrometry," *Journal of Chromatographic Science,* vol. 38, pp. 393-398, 2000.

[26] N. Rasmont, Linear Burn Rate of Green Ionic Liquid Multimode Monopropellant, Urbana, Illinois: University of Illinois at Urbana-Champaign, 2019.

[27] K. Popov, H. Rönkkömäki and L. H. J. Lajunen, "Critical Evalutation of Stability Constants of Phosphonic Acids," *Pure and Applied Chemistry,* vol. 73, no. 10, pp. 1641-1677, 2001.

[28] A. A. Schilt, Analytical Applications of 1,10-Phenanthroline and Related Compounds, Oxford: Pergamon Press, 1969.

[29] E. C. Constable and C. E. Housecroft, "The Early Years of 2,2'-Bipyridine - A Ligand in Its Own Lifetime," *MDPI Molecules,* vol. 24, no. 3951, 2019.

[30] N. L. Aluker, M. E. Herrmann and I. M. Suzdaltseva, "A Spectroscopic Study of Nitrate and Nitrite Salts and Their Aqueous Solutions," *Optics and Spectroscopy,* vol. 127, no. 6, pp. 906-911, 2019.

[31] V. A. Rafeev and Y. I. Rubtsov, "Kinetics and mechanism of thermal decomposition of hydroxylammonium nitrate," *Russian Chemical Bulletin,* vol. 42, no. 11, pp. 1811-1815, 1993.

[32] J. I. Artman and J. B. Ott, "Solid + liquid phase equilibria in the hydroxylammonium nitrate + water system," *Journal of Energetic Materials,* pp. 115-132, 1989.

[33] C. V. Krishnan, C. Creutz, H. A. Schwarz and N. Sutin, "Reduction Potentials for 2,2'-Bipyridine and 1,10-Phenanthroline Couples in Aqueous Solutions," *Journal of the American Chemical Society,* vol. 105, no. 17, pp. 5617-5623, 1983.

[34] M. R. Simond, K. Ballerat-Busserolles, Y. Coulier, L. Rodier and J.-Y. Coxam, "Dissociation Constants of Protonated Amines in Water at Temperatures from 293.15 K to 343.15 K," *Journal of Solution Chemistry,* vol. 41, pp. 130-142, 2011.

[35] J. Raaflaub, "Applications of Metal Buffers and Metal Indicators in Biochemistry," in *Methods of Biochemical Analysis, Volume 3*, Interscience Publishers, Inc., 1956, pp. 301-325.

[36] P. D. Garn, "An Examination of the Kinetic Compensation Effect," *Journal of Thermal Analysis,* vol. 7, pp. 475-478, 1975.

[37] J. Zsakó, "The Kinetic Compensation Effect," *Journal of Thermal Analysis,* vol. 9, pp. 101-108, 1976.

[38] T. B. Brill, P. E. Gongwer and G. K. Williams, "Thermal Decomposition of Energetic Materials. 66. Kinetic Composition Effects in HMX, RDX, and NTO," *Journal of Physical Chemistry,* vol. 98, no. 47, pp. 12242-12247, 1994.

[39] T. Ozawa, "A New Method of Analyzing Thermogravimetric Data," *Bulletin of the Chemical Society of Japan,* vol. 38, no. 11, pp. 1991-1886, 1965.

[40] J. H. Flynn and L. A. Wall, "A Quick, Direct Method for the Determination of Activation Energy from Thermogravimetric Data," *Journal of Polymer Science,* vol. 4, no. 1211, pp. 323-328, 1966.

[41] Sauerbrunn, S; Gill, P;, "Decomposition Kinetics Using TGA," TA Instruments, New Castle, DE, 1992.

[42] ASTM International, "Standard Test Method for Decomposition Kinetics by Thermogravimetry Using the Ozawa/Flynn/Wall Method," ASTM Committee on Thermal Measurements, 2016.

[43] S. Vyazovkin, A. K. Burnham, M. J. Criado, L. A. Pérez-Maqueda, C. Popescu and N. Sbirrazzuoli, "ICTAC Kinetics Committee Recommendations for Performing Kinetic Computations on Thermal Analysis Data," *Thermochimica Acta,* vol. 520, pp. 1-19, 2011.

APPENDIX A: COMPLEX PHOTOGRAPHS

Samples were made with approximately 100 ppm of copper in nitric acid, with Bipy added in varying mole ratios to the copper. As confirmed by the presented spectrophotometry results, Bipy complexing with copper appears a pale blue, shown in Figure 14.

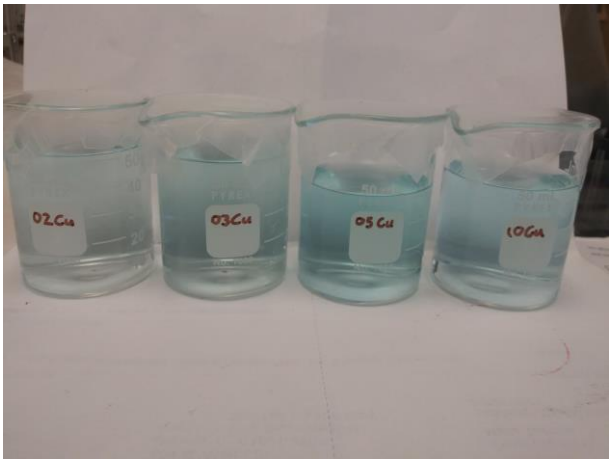

Figure 14. Photograph of samples with 100 ppm Cu with 2, 3, 5, and 10 times as many moles of Bipy added respectively, from left to right in HNO_3 solution.

Using the same procedure with 100 ppm iron and varying the mole ratio of Bipy added, samples are a deep red instead, shown in Figure 15. Chelate complexes with different metals absorb different wavelengths of light and appear different colors in solution. In the case of Bipy, copper complexes appear a pale blue and iron complexes appear red.

Figure 15. Photograph of samples with 100 ppm Fe with 1, 2, 3, 5, 7.5, and 10 times as many moles of Bipy added respectively, from left to right in HNO_3 solution.

The above samples in nitric acid are compared with HAN samples without any user-added metals. In Figure 16, a 90% aqueous HAN sample is compared with other 90% HAN samples with 0.05%, 0.1%, 0.5%, 1%, and 5% Bipy added. The pale red color indicates the presence of trace quantities of iron available to form complexes with the added Bipy. HAN with TEA or EDTA added does not change color and remains the same clear color as the 90% HAN sample in Figure 16. TEA and EDTA complexes with metals are not expected to change color in the visible spectrum.

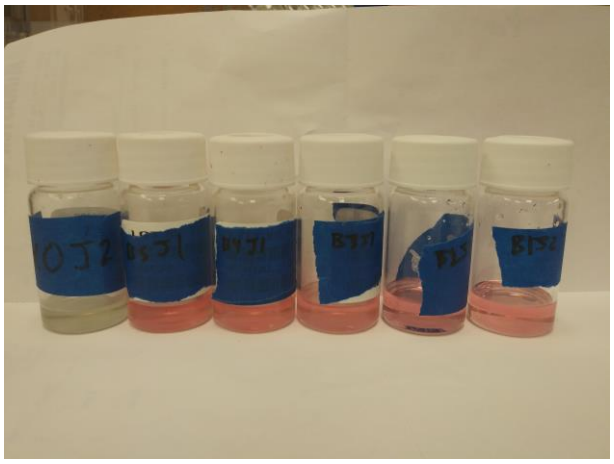

Figure 16. Photograph of 90% wt. HAN + water samples no additive, 0.05%, 0.1%, 0.5%, 1%, and 5% Bipy respectively, from left to right.

Following the same procedure as the added metal and Bipy to a nitric acid solution, copper and iron was added to a HAN solution. Figure 17 shows two of these samples compared with the same 1% Bipy sample as in Figure 16. Shown by the sample in the middle, when additional iron is added to HAN with Bipy added, the color of the solution is practically indistinguishable as reflected by the spectrophotometry results. When additional copper is added instead of iron, it forms complexes that appear pale blue which compete with the pale red of the iron complex to present as a pale purple solution. This visually confirms the presence of iron impurities and that they are complexed by Bipy added to these solutions.

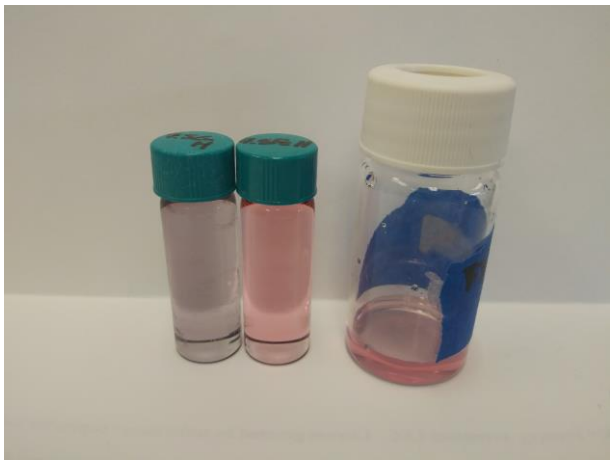

Figure 17. Photograph of samples with 7.5 mole ratio of Bipy:Cu and Bipy:Fe compared with 1% Bipy all in 90% HAN solution.

APPENDIX B: WATER CONTENT BY TGA

A TGA curve of an 80% aqueous HAN sample under a 10°C/min heating rate is shown in Figure 18 alongside the derivative of the mass response with respect to temperature. There are two mass loss events observed near 100°C and 175°C. An 80% aqueous HAN sample theoretically contains 20% water and 80% HAN by mass. The first event near 100°C drops the mass to about 80%, indicating that this first event is the water evaporating from the sample. This is like the 10% drop in mass of the 90% HAN sample shown in Figure 5. The second event near 175°C is the HAN decomposing to gaseous products and corresponds to the remaining 80% of the sample's mass. Because the peaks in mass loss rate for each step do not overlap to form a compound peak, the water evaporation step and the HAN decomposition step are observed to be independent of each other.

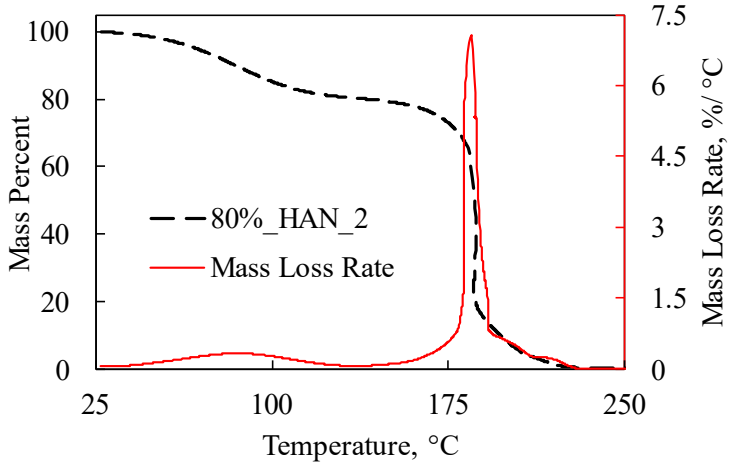

Figure 18: Sample dynamic TGA mass percent and derivative data of a 10°C/min constant rate ramp on a sample of 80% aqueous HAN.

After the water evaporation mass loss event, there is a 'plateau' before the start of the HAN decomposition event. Figure 19 shows a zoomed-in view of the water evaporation mass

loss event from Figure 18 and the subsequent plateau in mass. If it were truly a plateau, the mass loss rate would go to zero and there would be no mass loss after all the water evaporates and before the HAN begins to decompose. In the case of the TGA ramp at 10°C/min heating rate shown in Figure 18 and Figure 19, the mass loss rate does not drop completely to zero. However, the minimum mass loss rate between the two events can be used to estimate the mass lost in the first event. This method can be used to estimate the water content in HAN samples. The minimum rate between each mass loss event is 0.05827%/min at 135.7 degrees Celsius. At the same time, there is 80.27% of the sample's mass remaining. This measurement corresponds well to nearly all the expected 20.0% water in the sample having evaporated.

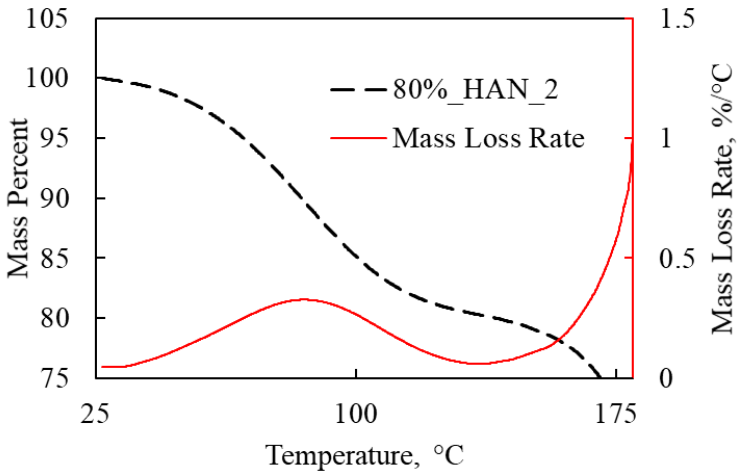

Figure 19: Sample dynamic TGA mass percent and derivative data of a 10°C/min constant rate ramp on a sample of 80% aqueous HAN, zoomed in on the water evaporation step.

Dynamic TGA data at constant heating ramps were acquired for samples of 80% aqueous HAN and 90% aqueous HAN. Data for each of these species are shown in Figure 20 and Figure 8 respectively. Samples of 80% HAN were tested at 10°C/min. This produced similar mass responses and thereby similar measurements of water content at 19.6 ± 0.3%. This is near the expected 20.0% but a slight underestimate. The underestimate may indicate some remaining water because of HAN's hygroscopicity. The 90% HAN samples were tested at varying heating

rates of 2, 5, 10, 15, and 20°C/min for the calculation of Arrhenius rate parameters. Data calculated from each dynamic TGA test are shown in Table 4.

For a faster heating rate, any given temperature-dependent mass loss event occurs at a higher temperature because there is a greater lag in the true temperature of the sample compared to the temperature-measuring thermocouple that sits in the gas adjacent to the sample. This is observed for both the water evaporation event and the HAN decomposition event in the data shown in Figure 8. Figure 21 shows a zoomed-in view of the water decomposition event and the subsequent plateau in mass from the data in Figure 8, showing that the mass does not flatten completely. The zoomed-in view also shows that even with more time between mass loss events due to a slower heating rate, the length of the plateau is not extended since the temperature where each mass loss event occurs is affected as well. Essentially, the entire thermogram including water evaporation, plateau, and HAN decomposition is shifted to the right, occurring at a higher temperature for a higher heating rate.

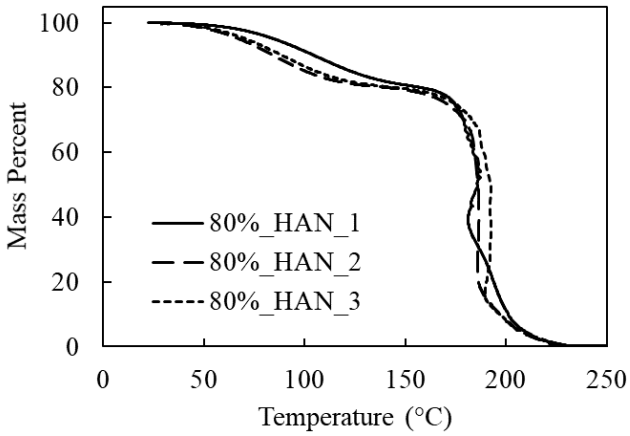

Figure 20: Dynamic TGA mass percent data of 80% aqueous HAN samples at 10°C/min constant rate ramps.

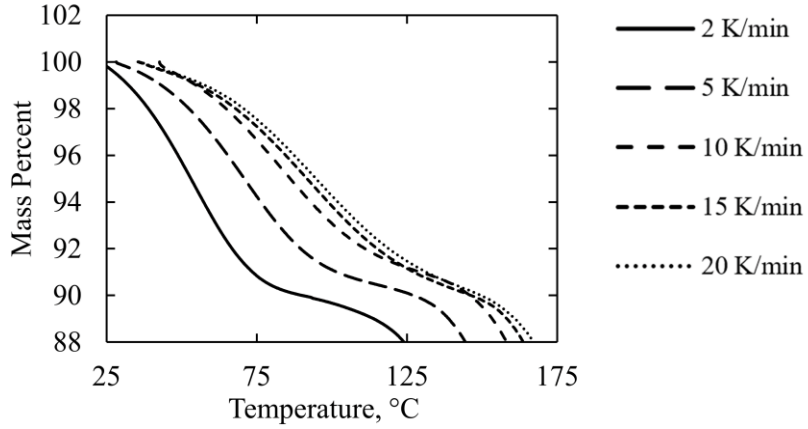

Figure 21: Dynamic TGA mass percent data of 90% aqueous HAN samples at 2, 5, 10, 15, and 20°C/min constant rate ramps, zoomed in on the water evaporation step.

Table 4. Dynamic TGA test initial masses and water contents.

Test ID	Initial Mass, mg	Theoretical Water Content	Water Content by TGA method
80%_HAN_1	38.87	20.0 %	19.32 %
80%_HAN_2	14.26	20.0 %	19.73 %
80%_HAN_3	17.31	20.0 %	19.74 %
90%HAN, 2K/min	14.77	10.0 %	10.12 %
90%HAN, 5K/min	16.00	10.0 %	9.55 %
90%HAN, 10K/min	16.17	10.0 %	8.95 %
90%HAN, 15K/min	15.34	10.0 %	9.82 %
90%HAN, 20K/min	14.13	10.0 %	9.64 %

Isothermal TGA methods are explored for their ability to extend the time between these two mass loss events. Isothermal TGA data of 90% aqueous HAN samples taken at a constant temperature of 75°C for 48 hours are shown in Figure 4. The sample is heated at 10°C/min to 75°C from room temperature, taking place in the first 6 minutes of the test followed by the isothermal hold for 48 hours. Within the first hour of the test water evaporates rapidly, then the

HAN decomposes more slowly for the remainder of the test. This is observed by the two approximately linear regions of high and low slope corresponding to water evaporation and HAN decomposition, respectively.

Three of the samples analyzed contain Bipy, TEA, and EDTA additives which are not expected to decompose at 75°C or contribute to the water content, therefore they can be ignored for water content analysis. The 1% additive content reduces the input water content by 1% from 10.0% to 9.9%.

Figure 22 shows a zoomed-in view of the first 120 minutes of the isothermal tests in Figure 4. It shows that there is a plateau after the water evaporation and before the HAN starts to slowly decompose. The mass loss rate minima occur near 60 minutes at a rate under 0.05%/min, which is lower than that observed in the dynamic TGA data. This means that more of the water has evaporated while less of the HAN has decomposed.

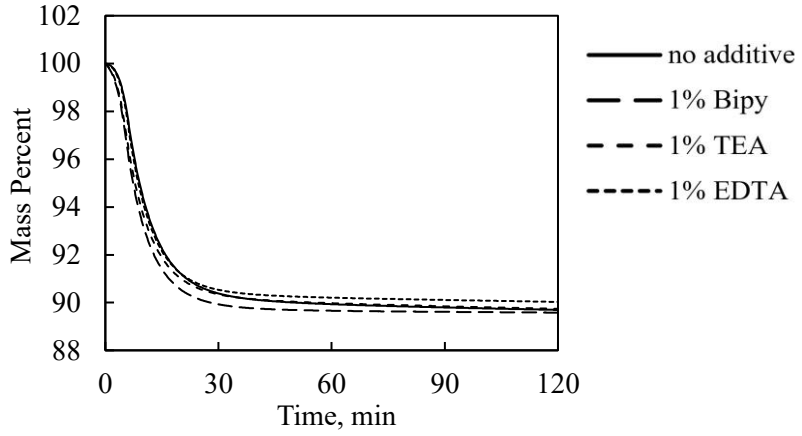

Figure 22: Isothermal TGA mass percent data of 90% aqueous HAN samples at 75°C, zoomed in on water evaporation event.

Initial masses, input water content, and water content measured by TGA in isothermal tests are shown in Table 5. In isothermal TGA tests, the initial mass is not expected to have any effect on the accuracy of the water content measurement but is included for completeness. For

aqueous HAN samples, the water content measured by isothermal TGA was within 0.44% of the expected value.

Table 5. 75°C Isothermal TGA test initial masses and water content measurements.

Test ID	Initial Mass, mg	Theoretical Water Content	Water Content by TGA method
HAN – no additive	33.28	10.0 %	10.06 %
1% Bipy	30.10	9.9 %	10.34 %
1% TEA	31.27	9.9 %	10.02 %
1% EDTA	29.18	9.9 %	9.80 %

If the evaporation of water and the decomposition of HAN are truly independent, then there are two different temperatures where each process occurs. If a sample containing HAN and water was held at a constant temperature between the temperature of water evaporation and the temperature of HAN decomposition, the water would evaporate, and the HAN would remain. This is not observed to be true in practice, where even at an intermediate temperature between those of water evaporation and HAN decomposition a non-zero rate of mass loss is observed. Therefore, for the most accurate determination of water content, an isothermal test at the minimum temperature where water evaporates in under an hour is recommended. This may occur at a lower temperature than the 75°C used in the isothermal tests presented here.